Photoproduction in Ultra-Peripheral Relativistic Heavy Ion Collisions at STAR

Boris Grube[1] for the STAR Collaboration

[1]Excellence Cluster Universe, Technische Universität München, Garching, Germany

In ultra-peripheral relativistic heavy ion collisions the beam ions scatter at impact parameters larger than the sum of their radii, so that they interact via long range electromagnetic forces. Due to the Lorentz-boost of the beam particles, the exchanged virtual photons have high energies and can induce the photoproduction of vector-mesons. We present recent results of the STAR experiment at RHIC on $\rho^0(770)$ production in Au-Au ultra-peripheral collisions at various energies. STAR has also observed the photoproduction of $\pi^+\pi^-\pi^+\pi^-$, which is related to the still poorly known excited states of the ρ^0.

1 Introduction

The electromagnetic field of a nucleus which is moving at relativistic velocities can be approximated by a flux of quasi-real virtual photons using the Weizsäcker-Williams approach [1]. The number of photons scales with the atomic charge Z squared, so that fast moving heavy nuclei create intense photon fluxes. Relativistic heavy ions may thus be used as photon sources or targets.

In Ultra-Peripheral relativistic heavy ion Collisions (UPCs) the long-range electromagnetic interactions are separated from the otherwise indistinguishable hadronic interactions by requiring impact parameters b larger than the sum of the nuclear radii R_A of the beam ions. Due to the large Lorentz-boosts of the beam particles, it is possible to study photonuclear reactions as well as photon-photon interactions at high energies in UPCs [2].

The photoproduction of vector mesons is a typical process in UPCs. A virtual photon, radiated by the "emitter" nucleus, fluctuates into a $q\bar{q}$ pair, which scatters elastically off the "target" nucleus and emerges as a real vector meson (cf. Fig. 1a). At high energies the scattering can be described in terms of soft Pomeron exchange. The cross section is strongly enhanced at low transverse momenta $p_T \lesssim 2\hbar/R_A$ of the produced meson, because the $q\bar{q}$ pair couples coherently to the entire nucleus. For these coherent processes the cross section depends on the nuclear form factor $F(t)$, where t is the squared four-momentum transfer to the target nucleus. For larger p_T the $q\bar{q}$ pairs couple to the individual nucleons within the target nucleus resulting in a smaller cross section which scales approximately with the mass number A modulo corrections for the nuclear absorption of the meson.

Because of the intense photon flux in the case of heavy beam ions, the photoproduction of vector mesons may be accompanied by Coulomb excitation of the beam particles. The excited ions decay mostly via neutron emission [3] which is a distinctive event signature that can be utilised in the trigger decision. In lowest order the vector meson photoproduction accompanied by mutual nuclear dissociation of the beam ions is a three-photon process. One

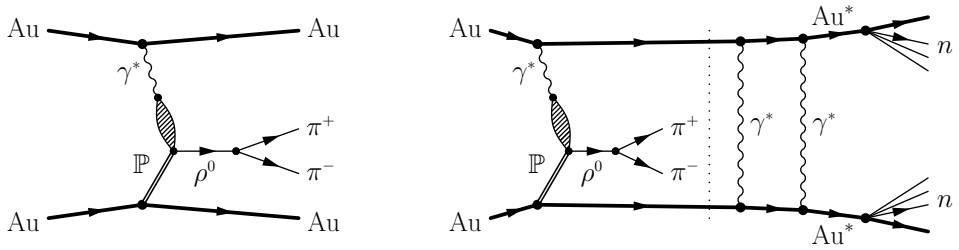

Figure 1: Schematic view of the photonuclear production of a $\rho^0(770)$ meson in an ultra-peripheral Au-Au collision and its subsequent decay into two charged pions. The meson is produced in the fusion processes of a virtual photon γ^* and a Pomeron $\mathbb{P}$. a) shows the exclusive reaction, b) the one with mutual Coulomb excitation of the beam ions and following neutron emission.

photon produces the vector meson and two additional photons excite the nuclei (see Fig. 1b). In good approximation all three photon exchanges are independent so that the cross section can be factorised [3]:

$$\sigma_{V,\,xn\,xn} = \int \mathrm{d}^2 b\,[1 - P_{\mathrm{had}}(b)] \cdot P_V(b) \cdot P_{xn,1}(b) \cdot P_{xn,2}(b),$$

where $P_{\mathrm{had}}(b)$ is the probability for hadronic interaction, $P_V(b)$ the probability to produce a vector meson V, and $P_{xn,i}(b)$ the probability that nucleus i emits x neutrons. Compared to exclusive photonuclear vector meson production, reactions with mutual Coulomb excitation have smaller median impact parameters.

In this paper we present recent results from the STAR experiment at the Relativistic Heavy Ion Collider (RHIC). The Solenoidal Tracker At RHIC (STAR) uses a large cylindrical Time Projection Chamber (TPC) [4] with 2 m radius and 4.2 m length, operated in a 0.5 T solenoidal magnetic field to reconstruct charged tracks. For tracks with pseudorapidity $|\eta| < 1.2$ and transverse momentum $p_T > 100$ MeV/c the tracking efficiency is better than 85 %. The UPC trigger is based on two detector systems: The two Zero Degree Calorimeters (ZDCs) [5] which sit at ± 18 m from the interaction point and measure neutral particles emitted in very forward direction. They have an acceptance close to unity for the neutrons originating from nuclear dissociation of the beam ions. The second trigger detector system used to select UPC events is the Central Trigger Barrel (CTB) [6]. It is an array of 240 plastic scintillator slats that surrounds the TPC and provides information about the charged-particle multiplicity.

Two basic types of trigger algorithms are used: The "topology" trigger requires a low overall charged-particle multiplicity and subdivides the CTB into four azimuthal quadrants. Events with coincident hits in the left and right quadrants are recorded thereby selecting roughly back-to-back pion pairs. The top and bottom quadrants are used to veto cosmic rays which otherwise could be reconstructed as unlike-sign particle pairs with zero transverse momentum and rapidity. Since there is no requirement on the energy deposit in the ZDCs, the "topology" data mainly contain exclusively produced vector mesons. In contrast to this the "minimum bias" trigger selects UPC events, where both beam ions dissociated by requiring coincident energy deposits in the ZDCs in addition to a low total charged-particle multiplicity in the

CTB.

In the offline analysis two- and four-prong events are selected by requiring two and four charged tracks, respectively, in the TPC to have zero net charge and to form a common (primary) vertex. All tracks are assumed to be pions. In order to suppress backgrounds from beam-gas interactions, peripheral hadronic interactions, and pile-up events in addition a low overall charged-track multiplicity is required. Backgrounds from pile-up events, beam-gas interactions, and — in the case of the two-prong sample — cosmic rays are reduced by selecting events with their primary vertex in a region close to the interaction diamond. Cosmic ray backgrounds in the two-prong "topology" sample are suppressed further by excluding events with rapidities $y_\rho \approx 0$. Due to the ZDC requirement in the "minimum bias" trigger, the cosmic ray background is nearly completely removed. Finally, coherent events are selected by requiring small transverse momenta of $p_T < 150$ MeV/c for the produced vector mesons.

2 Coherent Photoproduction of $\rho^0(770)$

There are at least three models that describe the production of $\rho^0(770)$ mesons in ultra-peripheral collisions: The model of Klein and Nystrand (KN) [7] uses the Vector Dominance Model (VDM) for the virtual photon and a classical mechanical approach for the scattering on the target nucleus, based on data from $\gamma\, p \to \rho^0(770)\, p$ experiments. The Frankfurt, Strikman, and Zhalov (FSZ) model [8] employs a generalised VDM to describe the virtual photon and a QCD Gribov-Glauber approach for the scattering. The model of Gonçalves and Machado (GM) [9] takes into account nuclear effects and parton saturation phenomena by using a QCD colour dipole approach.

The coherent cross section of $\rho^0(770)$ production accompanied by mutual nuclear dissociation of the beam ions $\sigma^{\rm coh}_{\rho,xnxn}$ is measured using "minimum bias" data. The ρ^0 yield is estimated by fitting the invariant mass peak of the acceptance corrected $m_{\pi^+\pi^-}$ distribution and extrapolating the result from the experimentally accessible rapidity range of $|y_\rho| < 1$ to the full solid angle using the KN model [7]. In Au-Au collisions at $\sqrt{s_{_{NN}}} = 200$ GeV the cross section was measured to be $\sigma^{\rm coh}_{\rho,xnxn} = 31.9 \pm 1.5_{\rm stat.} \pm 4.5_{\rm syst.}$mb; at $\sqrt{s_{_{NN}}} = 130$ GeV the value is $28.3 \pm 2.0_{\rm stat.} \pm 6.3_{\rm syst.}$mb [10].

Since the efficiency of the "topology" trigger is not well known, the total cross section $\sigma^{\rm coh}_{\rho,{\rm tot}}$ is estimated by applying coherent cross section ratios for different nuclear excitation states, which are extracted from the "topology" data, to the cross section values for mutual excitation. This way the total coherent ρ^0 production cross section is measured to be $530 \pm 19_{\rm stat.} \pm 57_{\rm syst.}$mb at $\sqrt{s_{_{NN}}} = 200$ GeV and $460 \pm 220_{\rm stat.} \pm 110_{\rm syst.}$mb at $\sqrt{s_{_{NN}}} = 130$ GeV [10]. In Fig. 2a the total cross sections and the cross sections with mutual nuclear dissociation are compared to the KN model predictions.

Figure 2b shows the measured total coherent ρ^0 production cross section as a function of rapidity and compares to the various model predictions. Due to the limited experimentally accessible rapidity range of $|y_\rho| < 1$, it is not possible to discriminate the models based on the shape of their rapidity distribution. Considering the cross section values, the KN model agrees best with the data.

In ρ^0 production an interesting interference phenomenon is caused by the fact that the ρ^0 is produced close ($\mathcal{O}(1$ fm$)$) to the target nucleus and that the emitter and the target nucleus are indistinguishable. Because the impact parameter is larger than the sum of the nuclear radii of the projectiles, the system essentially acts like a two-slit interferometer with slit separation

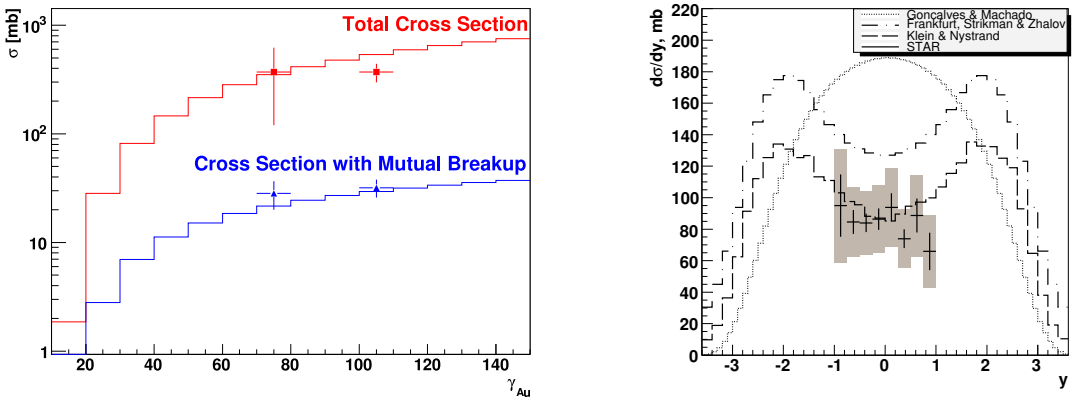

a) b)

Figure 2: a) Energy dependence of the total coherent cross section (red) and the one with mutual nuclear dissociation (blue) in comparison to the KN model predictions (continuous histogram). b) Comparison of the measured total cross section for coherent ρ^0 production with theoretical predictions [10]. The vertical line at each point shows the statistical error. The shaded area displays the sum of statistical and systematic errors. The dashed line represents the KN [7], the dash-dotted line the FSZ [8], and the dotted one the GM model [9].

$|\vec{b}|$. Either nucleus A emits a virtual photon which scatters off nucleus B or vice versa. The two indistinguishable processes are related by parity transformation and, since the ρ^0 has negative intrinsic parity, the amplitudes have to be subtracted [11]:

$$\sigma(\vec{p}_T, \vec{b}, y_\rho) = \left| A(p_T, b, y_\rho) - A(p_T, b, -y_\rho)\, e^{i\vec{p}_T \cdot \vec{b}} \right|^2$$

At mid-rapidity $A(p_T, b, y_\rho) \approx A(p_T, b, -y_\rho)$ so that the above equation simplifies to

$$\sigma(\vec{p}_T, \vec{b}, 0) = 2\,|A(p_T, b, 0)|^2 \left[1 - \cos(\vec{p}_T \cdot \vec{b})\right]$$

The interference is destructive for transverse momenta $p_T \lesssim \hbar/\langle b \rangle$. Figure 3 shows the $t(\approx p_T^2)$ distribution, which is roughly exponential at larger t, but has a significant downturn for $t < 0.0015$ (GeV/c)^2, consistent with the Monte-Carlo simulation that includes the interference effect.

The flight path $\beta\gamma c\tau$ of the produced ρ^0 is much smaller than the impact parameter so that the ρ^0 decays at two well-separated points in space-time. This means that the amplitudes overlap and interfere only *after* the decay and that the interference must involve the $\pi^+\pi^-$ final state. Interference is only possible, if the final state wave function is entangled, nonlocal, and not factorisable into individual $\pi^\pm$ wave functions.

The strength of the interference is extracted from the data by fitting the t distribution with the function

$$\frac{\mathrm{d}N}{\mathrm{d}t} = a\, e^{-kt} \left[1 + c\,(R(t) - 1)\right]$$

where k is the slope parameter and c the spectral modification parameter that measures the interference. A value of $c = 0$ would correspond to no interference, a value of $c = 1$ to the interference predicted by the KN model [7, 11]. The deviation of the t distribution from the exponential shape due to the interference effect is parameterised by the function $R(t)$ which is determined from the ratio of the simulated t spectrum with and without interference. The measured spectral modification parameter of $87 \pm 5_{\mathrm{stat.}} \pm 8_{\mathrm{syst.}}$% shows that the interference is significant [12], which means that the $\pi^+\pi^-$ final state wave function retains amplitudes for all possible ρ^0 decays, long after the decay occurred. The system is thus an example of the Einstein-Podolsky-Rosen paradox [16] with continuous variables momentum and position.

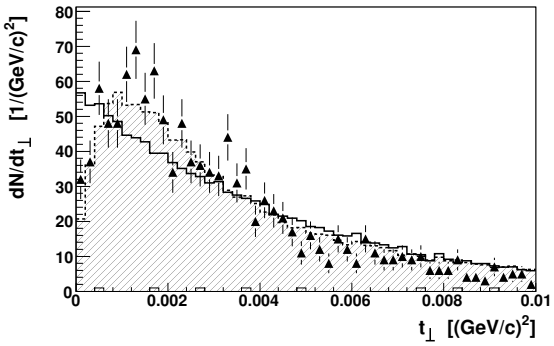

Figure 3: Uncorrected t spectrum of ρ^0 in the rapidity range $|y_\rho| < 0.5$ for the "minimum bias" data [12]. The points represent the data. The dashed (filled) histogram is a simulation that includes the interference effect, whereas the solid histogram is a simulation without interference.

3 Coherent Photoproduction of $\pi^+\pi^-\pi^+\pi^-$ Final States

Coherent $\pi^+\pi^-\pi^+\pi^-$ production in ultra-peripheral collisions accompanied by mutual nuclear dissociation of the beam ions was measured in Au-Au collisions at $\sqrt{s_{NN}} = 200$ GeV using the "minimum bias" data. The transverse momentum spectrum of the neutral four-prongs exhibits an enhancement at low p_T characteristic for coherent production (cf. Fig. 4a). The data show a broad peak in the $\pi^+\pi^-\pi^+\pi^-$ invariant mass distribution (see Fig. 4b), similar to what was seen in earlier fixed-target photoproduction experiments [13, 14]. This peak is usually attributed to the excited ρ^0 states $\rho(1450)$ and $\rho(1700)$. However, the exact nature of these states is still controversial.

The $\pi^+\pi^-\pi^+\pi^-$ invariant mass distribution was fitted with a S-wave Breit-Wigner modified by a phenomenological Ross-Stodolsky factor [15]:

$$f(m) = A \cdot \left(\frac{m_0}{m}\right)^n \cdot \frac{m_0^2\Gamma_0^2}{(m_0^2 - m^2)^2 + m_0^2\Gamma_0^2} + f_{\mathrm{BG}}(m) \qquad (1)$$

The non-interfering background f_{BG} was parameterised by a second order polynomial which was extracted from the invariant mass distribution of $+2$ or -2 charged four-prongs. Taking into account the experimental acceptance, the fit yields a resonance mass of 1540 ± 40 MeV/c^2 and a width of 570 ± 60 MeV. The Ross-Stodolsky exponent has a value of $n = 2.4 \pm 0.7$, however, mass and width depend strongly on the value of n.

Using the acceptance-corrected $\pi^+\pi^-\pi^+\pi^-$ yield from the above fit and the respective $\rho^0(770)$ yield from the $\pi^+\pi^-$ invariant mass distribution the cross section ratio $\sigma^{\mathrm{coh}}_{4\pi,xnxn}/\sigma^{\mathrm{coh}}_{\rho,xnxn}$ is estimated to be 13.4 ± 0.8 %, where again the KN model [7] was used to extrapolate from the experimentally accessible rapidity region $|y| < 1$ to the full solid angle. Using the measured

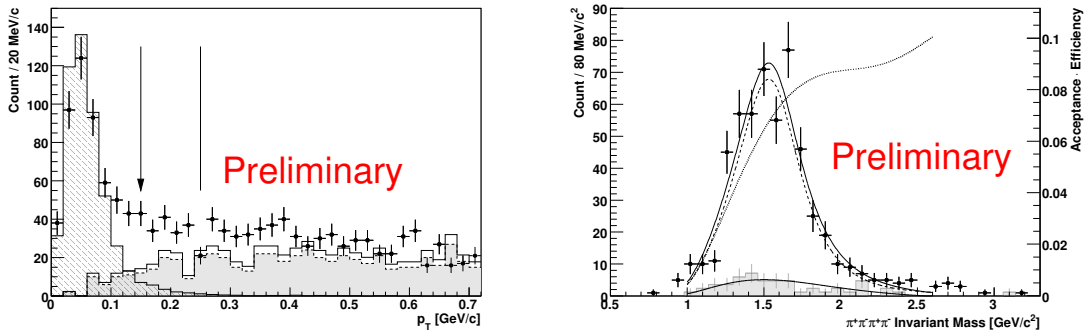

a) **b)**

Figure 4: a) $\pi^+\pi^-\pi^+\pi^-$ transverse momentum distribution: At low transverse momenta the four-prong couples coherently to the entire nucleus leading to a strong enhancement of the cross section. The hatched filled histogram shows the expected distribution from simulation. The background for the coherent part is estimated from +2 or −2 charged four-prong combinations by normalising their p_T distribution (gray filled histogram) to that of the neutral four-prongs in the region of $p_T > 250$ MeV/c (vertical line) yielding the unfilled histogram. b) Invariant mass distribution of coherently produced $\pi^+\pi^-\pi^+\pi^-$: The points represent the data, the gray filled histogram is the background estimated from charged four-prongs. The thick black line shows the fit of the modified S-wave Breit-Wigner of Eq. (1) on top of a second order polynomial background (thin black line) taking into account the detector acceptance in the region $|y| < 1$ (rising dotted line). The dashed curve represents the signal curve without background.

coherent ρ^0 production cross section $\sigma^{\rm coh}_{\rho,xn,xn}$ the $\pi^+\pi^-\pi^+\pi^-$ production cross section is 4.3 ± 0.3 mb.

Figure 5a shows that $\pi^+\pi^-\pi^+\pi^-$ events mainly consist of a low mass $\pi^+\pi^-$ pair accompanied by a $\rho^0(770)$. This motivated the Monte-Carlo decay model $\rho' \to \rho^0(770)\ f_0(600)$ which is used to estimate the acceptance corrections. As can be seen in Fig. 5a this model reproduces the data well.

In photoproduction on carbon targets the ρ' was seen not only in the $\pi^+\pi^-\pi^+\pi^-$ decay mode, but also in $\pi^+\pi^-$ final states [14]. Figure 5b shows the high mass region of the measured $m_{\pi^+\pi^-}$ spectrum. In order to suppress backgrounds, in particular cosmic rays, tighter cuts are applied. The data do not show any significant enhancement around 1540 MeV/c^2.

4 Summary

STAR has measured photonuclear production of $\rho^0(770)$ in ultra-peripheral relativistic heavy ion collisions. The measured cross sections agree with model predictions. STAR also measured for the first time the interference effect in ρ^0 production which indicates that the decoherence induced by the ρ^0 decay is small and that the $\pi^+\pi^-$ final state wave function is entangled and nonlocal. In addition STAR has observed coherent photoproduction of $\pi^+\pi^-\pi^+\pi^-$ final states in UPCs. The $\pi^+\pi^-\pi^+\pi^-$ invariant mass spectrum exhibits a broad peak around 1540 MeV/c^2 and no corresponding enhancement is seen in the $m_{\pi^+\pi^-}$ distribution. The coherent $\pi^+\pi^-\pi^+\pi^-$ production cross section is 13.4 ± 0.8 % of that of the $\rho^0(770)$ meson.

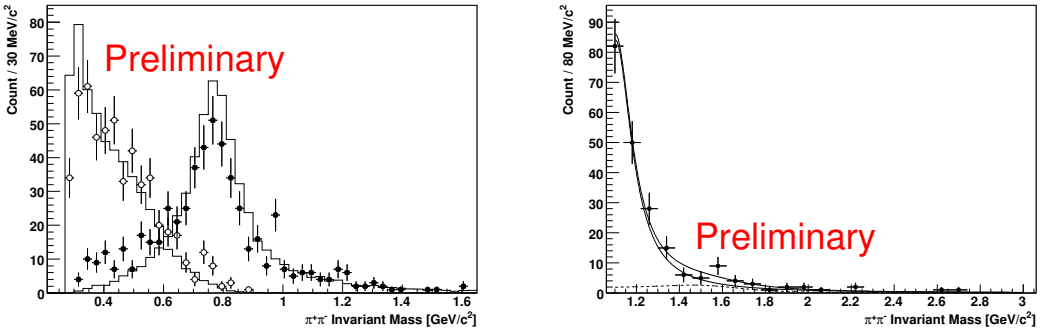

a) **b)**

Figure 5: a) Invariant Mass distribution of two-pion subsystems: The open circles show the measured invariant mass spectrum of the lightest $\pi^+\pi^-$ pair in the event. The filled circles represent the invariant mass distribution of the $\pi^+\pi^-$ that is recoiling against the lightest pair. The spectrum exhibits a clear peak in the $\rho^0(770)$ region. The solid line histograms show the prediction from simulation assuming the relative S-wave decay $\rho' \to \rho^0(770)\ f_0(600)$. b) High mass region of the $m_{\pi^+\pi^-}$ spectrum with tighter cuts applied in order to suppress background: The points represent the data. No significant enhancement is seen in the region around 1540 MeV/c^2 where the $\pi^+\pi^-\pi^+\pi^-$ invariant mass spectrum exhibits a peak.

References

[1] C. F. von Weizsäcker, Z. Phys. **88**, 612 (1934); E. J. Williams, Phys. Rev. **45**, 729 (1934).

[2] G. Baur, K. Hencken, D. Trautmann, S. Sadovsky, and Yu. Kharlov, Phys. Rept. **364**, 359 (2002); F. Krauss, M. Greiner, and G. Soff, Prog. Part. Nucl. Phys. **39**, 503 (1997); C. A. Bertulani, S. R. Klein, and J. Nystrand, Ann. Rev. Nucl. Part. Sci. **55**, 271 (2005); A. J. Baltz *et al.*, Phys. Rept. **458**, 1 (2008).

[3] A. J. Baltz, S. R. Klein, and J. Nystrand, Phys. Rev. Lett. **89**, 012301 (2002); G. Baur, K. Hencken, A. Aste, D. Trautmann, and S. R. Klein, Nucl. Phys. **A729**, 787 (2003).

[4] M. Anderson *et al.*, Nucl. Intrum. Methods **A499**, 659 (2003); **A499**, 679 (2003).

[5] C. Adler *et al.*, Nucl. Intrum. Methods **A470**, 488 (2001).

[6] F. S. Bieser *et al.*, Nucl. Intrum. Methods **A499**, 766 (2003).

[7] S. Klein and J. Nystrand, Phys. Rev. C **60**, 014903 (1999).

[8] M. Frankfurt, M. Strikman and M. Zhalov, Phys. Lett. **B537**, 51 (2002); Phys. Rev. C **67**, 034901 (2003).

[9] V. P. Gonçalves and M. V. T. Machado, Eur. Phys. J. **C40**, 519 (2005).

[10] C. Adler *et al.*, Phys. Rev. Lett. **89**, 272302 (2002); B. I. Abelev *et al.*, Phys. Rev. C **77**, 34910 (2008).

[11] S. R. Klein and J. Nystrand, Phys. Rev. Lett. **84**, 2330 (2000); Phys. Lett. A308, 323 (2003)

[12] B. I. Abelev *et al.*, Phys. Rev. Lett. **102**, 112301 (2009).

[13] H. H. Bingham *et al.*, Phys. Lett. **41B**, 635 (1972)); P. Schacht, I. Derado, D. C. Fries, J. Park, and D. Yount, Nucl. Phys. **B81**, 205 (1974); G. Alexander, O. Benary, J. Gandsman, D. Lissauer, A. Levy, Y. Oren and L. M. Rosenstein, Phys. Lett. **57B**, 487 (1975); D. P. Barber *et al.*, Z. Phys. **C4**, 169 (1980); D. Aston *et al.*, Nucl. Phys. **B189**, 15 (1981); M. Atkinson *et al.*, Z. Phys. **C26**, 499 (1985).

[14] M. S. Atiya *et al.*, Phys. Rev. Lett. **43**, 1691 (1979).

[15] M. Ross and L. Stodolsky, Phys. Rev. **149**, 1172 (1966).

[16] A. Einstein, B. Podolsky, and N. Rosen, Phys. Rev. **47**, 777 (1935)